Eur. Phys. J. A (2025) 61:142
https://doi.org/10.1140/epja/s10050-025-01609-2

THE EUROPEAN PHYSICAL JOURNAL A

Regular Article - Experimental Physics

Total cross sections of the ^{87}Rb(p, γ)^{88}Sr reaction measured via in-beam gamma-ray spectroscopy

Svenja Wilden [a], **Benedikt Machliner** [b], **Martin Müller** [c], **Andreas Zilges** [d]

Institute for Nuclear Physics, University of Cologne, Zülpicher Straße 77, 50937 Cologne, Germany

Received: 17 December 2024 / Accepted: 1 June 2025

Communicated by Navin Alahari

Abstract The ^{87}Rb(p, γ)^{88}Sr reaction was measured for the first time at astrophysically relevant energies in an in-beam experiment at the high-efficiency HPGe γ-ray spectrometer HORUS at the University of Cologne. To determine total cross sections of the ^{87}Rb(p, γ)^{88}Sr reaction, proton beams at six different energies between E_p = 2.0 MeV and 5.0 MeV were provided by a 10 MV FN tandem accelerator, spanning nearly the entire Gamow window relevant for the astrophysical γ-process. These total experimentally obtained cross sections were then compared to calculations performed using the TALYS 2.0 code. In comparison, the measured total cross-sections are found to be lower than those predicted by different models used as input parameters for the TALYS 2.0 code for E_p = 2.0 MeV to 3.5 MeV.

1 Introduction

The majority of nuclei heavier than iron are produced via neutron capture processes. These processes bypass the so-called p-nuclei, a set of 35 stable, neutron-deficient nuclei [1]. The p-process describes a variaty of processes that account for the production of the p-nuclei. One of these is the γ-process which is mainly responsible for producing p-nuclei via different combinations of photodisintegration reactions such as (γ, p), (γ, n) and (γ, α). The number of involved reactions for describing the synthesis of p-nuclei is often higher than 10 000. The most favoured sites for this process, where the required temperatures of 2 GK to 3 GK for photodisintegration reactions are reached, are O-Ne layers of type II supernovae [2,3].

However, lighter p-nuclei in the $A \approx 90$ mass region, such as ^{92}Mo, are significantly underproduced [4]. A process that has been proposed to resolve this issue is the νp-process [5]. The p-nuclide ^{92}Mo lies in the N = 50 isotonic chain and shields ^{92}Nb, an extinct radionuclide, from being produced in the rp- and νp-processes [6], if one neglects (n, p)-processes. Recently, the influence of exploding massive stars has been discussed [7].

As the ^{87}Rb(p,γ) reaction is also located in the $A \approx 80-100$ mass region as five of the p-nuclei and as ^{92}Mo in the N = 50 isotonic chain, the results might help to understand the production mechanisms of those and help to improve theoretical model calculations by constraining the cross sections and the input parameters in this mass region relevant for the p-process. The latter is crucial since statistical model calculations are often the only way to predict the cross sections for all the reactions involved in the huge network of reactions. As sensitivity studies show, there is a strong (γ, n) and (γ, p) flux towards the N = 50 isotonic chain followed by a series of (γ, p) photodisintegrations [8].

When calculating the stellar reaction rates from cross-sections it needs to be taken into account that due to high temperatures in a stellar plasma, a considerable thermal population of excited states is expected. However, the cross-sections measured in the laboratory are only on the ground states, why the ground-state contributions to the stellar rates need to be known. Combining theory and experimental data can be used to calculate the stellar reaction rate, if there is a contribution from excited states. Since the ground-state contributions are in general higher, if not ≈ 1, for the reaction direction with positive Q-value depending on the temperature, measurement of these reactions, as in our case (p, γ) instead of (γ, p), help to constrain the stellar reaction rates more precisely [6,9].

An increased production of ^{87}Rb and ^{88}Sr, with +47% and +7% respectively, has been found in massive-star mod-

[a] e-mail: swilden@ikp.uni-koeln.de (corresponding author)
[b] e-mail: bmachli@ikp.uni-koeln.de
[c] e-mail: mmueller@ikp.uni-koeln.de
[d] e-mail: zilges@ikp.uni-koeln.de

Published online: 19 June 2025

els using new neutron-capture cross sections on Kr-isotopes, which also leads to an increase of +24% for the p-nucleus ^{84}Sr during the O-shell burning [10]. During the C-O shell merger, the temperature is about 2.5 GK and ^{87}Rb and ^{88}Sr are abundant, which indicates, that a better understanding of the ^{87}Rb(p, γ)^{88}Sr or its inverse reaction, can as well help to constrain the stellar reaction rates for ^{84}Sr since ^{87}Rb and ^{84}Sr are linked by a sequence of reactions [11,12].

2 Experimental setup and method

The ^{87}Rb(p, γ)^{88}Sr reaction was investigated at the 10 MV FN tandem accelerator at the University of Cologne's Institute for Nuclear Physics, Germany. The HORUS γ-ray spectrometer, which is equipped with a dedicated target chamber for nuclear astrophysics experiments, was used for the investigation of the reaction [13]. Fourteen HPGe detectors were employed, positioned at the six faces and eight vertices of a cube. Six of the HPGe detectors were equipped with BGO shields for active Compton suppression. The current was read out at the target, the chamber and a Faraday cup situated further downstream behind the target. To prevent δ electrons from exiting the chamber, a suppression voltage of −400 V was applied to it.

2.1 Target properties

Due to the low melting point of pure rubidium of only 39.3°C, rubidium carbonate (Rb_2CO_3) with a melting point of 837°C was used. The target, with an isotopic enrichment in ^{87}Rb of 99.2(1)%, was produced by evaporating Rb_2CO_3 onto a gold backing in our in-house target laboratory. The gold backing with a thickness of 90 mg/cm^2 was used to stop the beam to avoid further beam induced background due to widening of the beam behind the target. In the following, this target will be referred to as T_1. After the experiment, Rutherford Backscattering Spectrometry (RBS) [14] was performed at the RUBION facility in Bochum, Germany [15], to determine the Rb target thickness. The results of this measurement indicated that gold from the backing had diffused into the Rb_2CO_3 layer during irradiation, thereby making it more challenging to determine the thickness for T_1, as can be seen in Fig. 1. The thickness of a second similar target of Rb_2CO_3, in the following denoted as T_2, that had not been exposed to a beam prior to this experiment, was determined to be 642(64) μg/cm^2 and showed no gold admixture visible in the RBS spectra. Its gold backing has a thickness of 85 mg/cm^2. Note, that the thickness of each gold backing was not measured via RBS but given after the target production, since it solely needs to be thick enough to stop the beam. In a subsequent experiment, T_2 was irradiated with protons at $E_p = 3.5$ MeV. Consequently, the thickness of

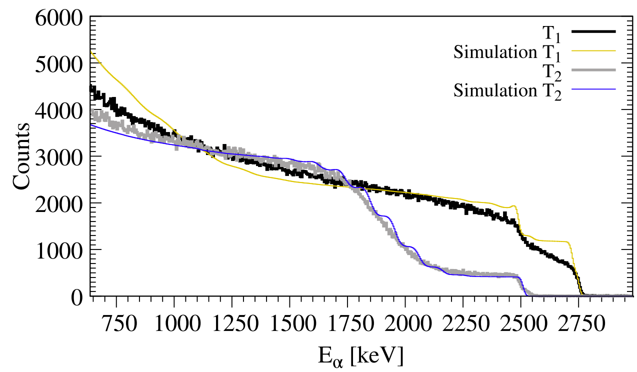

Fig. 1 Relevant part of the RBS spectra measured at the RUBION facility in Bochum, Germany [15], to determine the Rb target thickness for the targets T_1 and T_2. The spectra are well reproduced by simulations performed with SIMNRA [16]. T_1 displays an additional layer that is not present in T_2. The simulation of this layer proved to be a significant challenge. Consequently, the method outlined in the text was employed to determine the thickness of T_1

T_1 could be determined by normalizing the reaction yield for the ^{87}Rb(p,n) ^{87}Sr reaction obtained with T_1, at the same beam energy, to that obtained with T_2. This leads to the following equation:

$$\frac{N_{\gamma_i,2}}{N_{p_2}\cdot N_{T_2}} = \frac{N_{\gamma_i,1}}{N_{p_1}\cdot N_{T_1}} \\ \Leftrightarrow N_{T_1} = \frac{N_{\gamma_i,1}}{N_{\gamma_i,2}}\cdot\frac{N_{p_2}}{N_{p_1}}\cdot N_{T_2}, \tag{1}$$

where $N_{\gamma_i,j}$ is the γ-ray yield observed in the detectors placed at 90°, N_{p_j} is the number of projectiles, N_{T_j} is the number of target nuclei per area with $j \in \{1, 2\}$ and i denotes the used γ-ray transitions. The effective thickness of T_1 has thus been determined to be 727(72) μg/cm^2.

2.2 Beam properties

During the continuous irradiation of the ^{87}Rb target nuclei with protons of different energies $E_{c.m.}$ as given in Tab. 1, highly excited compound nuclei are formed with an excitation energy of

$$E_x = E_{c.m.} + Q, \tag{2}$$

where Q is the Q value of 10 612.8 keV for the radiative proton-capture reaction on ^{87}Rb [17] and $E_{c.m.}$ denotes the center-of-mass-energy. The effective proton-beam energy assuming an energy loss of ΔE in the target is given by

$$E_{\text{eff}} = E_p - \frac{\Delta E}{2}, \tag{3}$$

Table 1 The detailed beam characteristics for the different effective proton-beam energies E_{eff}, where $E_{c.m.}$ denotes the center-of-mass-energy, I denotes the total current and t denotes the irradiation duration for the in-beam measurement

E_{eff} [MeV]	$E_{c.m.}$ [MeV]	I [nA]	t [h]
1.970(23)	1.947(23)	620(31)	14.8
2.776(23)	2.744(23)	610(31)	20.3
3.480(22)	3.440(22)	430(22)	9.9
3.982(22)	3.936(22)	360(18)	11.8
4.483(22)	4.432(22)	170(9)	8.2
4.984(22)	4.928(22)	140(7)	15.6

which has been used to calculate the center-of-mass-energy $E_{c.m.}$. Here, E_p is the proton-beam energy provided by the accelerator. SRIM [18] was used to calculate the average energy loss ΔE in the target, which ranges between 34 keV to 64 keV depending on the proton-beam energy. If statistics are high enough, $E_{c.m.}$ can also be determined using prompt γ rays and the formula

$$E_{c.m.} = E_\gamma - Q + E_{state}, \tag{4}$$

where E_γ is the energy of the prompt γ ray and E_{state} is the energy of the state that is populated by the prompt γ-ray transition. With this knowledge, the offset of the proton-beam energy from the accelerator can be estimated. For the uncertainty of the beam energy we assume 20 keV. The uncertainty of the energy loss in the target is the standard deviation of the SRIM [18] simulation and is almost insignificant compared to the other uncertainties. More details can be found in Ref. [13].

The de-excitation of the compound nucleus was investigated via high-resolution in-beam γ-ray spectroscopy to determine total cross sections for six different proton-beam energies between $E_p = 2$ MeV and $E_p = 5$ MeV. These proton-beam energies have been selected to cover the region of the astrophysically relevant Gamow window for the ^{87}Rb(p, γ)^{88}Sr reaction, which lies between 1.28 MeV and 3.17 MeV at a temperature of $T = 3.0$GK.

The proton-beam energy, proton current, and irradiation time details for the six measured beam energies can be found in Tab. 1. Note that the current is increased with decreasing beam energy in order to partly compensate for the decreasing cross section. This was possible because with smaller beam energy the heat deposition in the target backing, which stops the beam, is smaller and the rate of undesired reactions, and especially the neutron production, is also reduced.

2.3 Spectra

Accurate knowledge of the full-energy peak efficiency for γ rays up to 16 MeV is required for determining total and partial cross sections. The efficiency of the low-energy part, up to 2.5 MeV, has been calibrated using a ^{226}Ra standard calibration source. By in addition using ^{56}Co and ^{66}Ga standards the detection efficiency of γ-rays can be determined precisely up to an energy of 4.8 MeV. The half-lives of these sources are 77.2 days [20] and 9.3 h [21], respectively. Fitting the efficiencies determined from these standards with a function of the form

$$\epsilon\left(E_\gamma\right) = a \cdot \exp\left(-b \cdot E_\gamma\right) + c \cdot \exp\left(-d \cdot E_\gamma\right) \tag{5}$$

leads to the full-energy peak efficiencies. This function is then used to extrapolate up to γ-ray energies of up to 16 MeV, where the uncertainty of the full-energy peak efficiency is about 12% in contrast to the uncertainty of 2% at $E_\gamma = 1.3$ MeV. For this experiment the total detection efficiency of HORUS is about 2.2% at $E_\gamma = 1.3$ MeV.

The digital data acquisition that is used at the HORUS γ-ray spectrometer consists of two CAEN S.p.A. V1782 digitizers for which details can be found in Refs. [22,23]. The events are stored in ROOT-tree format.

A schematic illustration of the reaction and the γ decays to the ground state that have been observed in ^{88}Sr [19] are shown in Fig. 2.

3 Data analysis

The experimental yield $Y(E_\gamma)$ of the ^{87}Rb(p, γ)^{88}Sr reaction is obtained by determining the peak volume for each ground-state transition visible in the γ-ray spectra. Two typical spectra are shown in Fig. 3 for beam energies of $E_p = 2.0$ MeV and $E_p = 5.0$ MeV with irradiation times of 14.8 h and 15.6 h, respectively. Given that ^{87}Rb has no stable isotopic neighbours, the only competing reaction at these energies is ^{87}Rb(p,n)^{88}Sr. As expected, for a proton-beam energy of 2.0 MeV the contribution of the (p, n) reaction is significantly lower than for higher beam energy. This behavior is consistent with statistical model calculations performed using the TALYS 2.0 code [24], which predict a reduction by approximately a factor of 2000. Other transitions being visible stem from proton-induced reactions on ^{197}Au used as

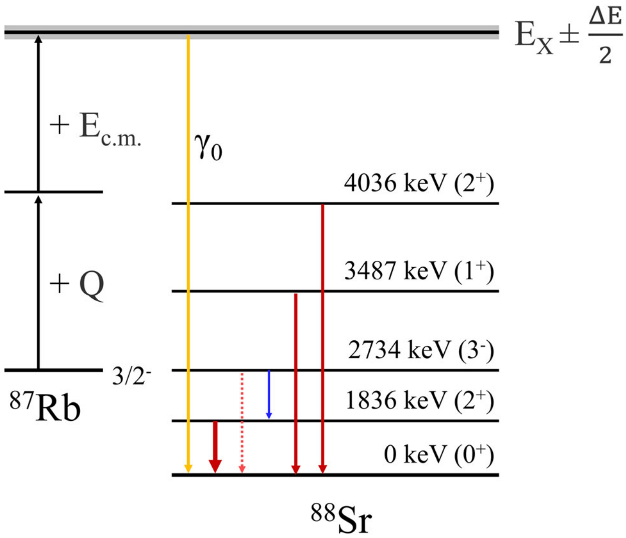

Fig. 2 Schematic illustration of the proton-capture reaction on ^{87}Rb. The highly excited compound nucleus contains many unresolved resonances and has a width of about $\frac{\Delta E}{2}$, with ΔE being the energy loss. It can de-excite directly to the ground state of ^{88}Sr via a single transition (γ_0) or into excited states followed by various γ-ray cascades. Here, only states for which the ground-state transition was observed are displayed. The thicker the arrow the more dominant are the branchings. The data are taken from Ref. [19]

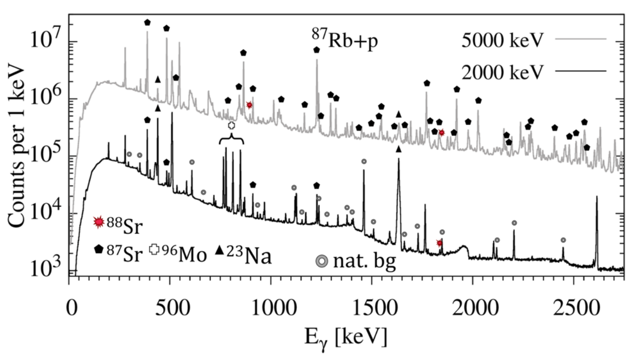

Fig. 3 Comparison of γ-ray spectra obtained at beam energies of E_p = 2000 keV and 5000 keV. The different symbols represent the different origins of some peaks. A noticeable decrease in the (p, n) reaction cross section with decreasing energy is observed. Note that the ^{96}Mo lines stem from an old contamination inside the target chamber and not the target itself

backing. Since the cross sections are very small, especially at low beam energies, lines resulting from natural background radiation, such as that of, e.g., ^{40}K and ^{226}Ra, as well as from target contaminants like ^{23}Na, are clearly visible. The ^{96}Mo lines stem from a contamination inside the target chamber caused by a previous experiment. At higher beam energies, however, transitions in the (p, n) product ^{87}Sr dominate the γ-ray spectra.

In order to obtain the total cross sections, it is necessary to determine the peak volumes of all ground-state transitions

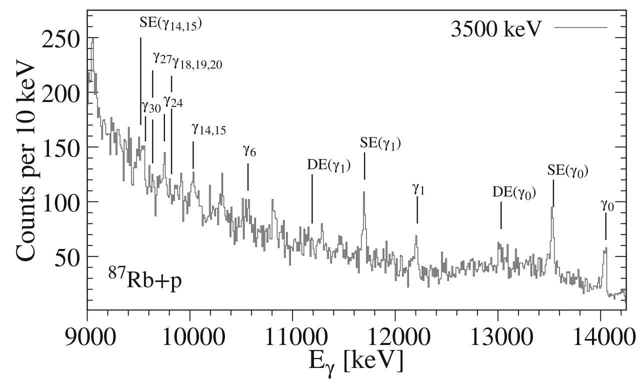

Fig. 4 High energy part of the in-beam γ-ray spectrum for the detectors placed at 90° for a proton-beam energy of E_p = 3.5 MeV. The positions of primary γ-rays to certain discrete states in ^{88}Sr are labeled

for each beam energy. Figure 2 shows the relevant part of the level scheme in ^{88}Sr for this analysis.

3.1 γ-ray spectra

The γ-ray line at E_γ = 1836 keV from the ^{87}Rb(p,γ) reaction is partially contaminated with the de-excitation of the excited $\frac{3}{2}^+$ state at E_x = 3602 keV stemming from the ^{87}Rb(p,n) reaction. This level de-excites to the $\frac{5}{2}^+$ level at E_x = 1770 keV with E_γ = 1832 keV [25]. This line is clearly visible in the γ-ray spectra for E_p = 5.0 MeV and E_p = 4.5 MeV and makes the determination of the number of γ-ray transitions stemming from the proton-capture reaction for the 1836 keV transition more challenging.

The de-excitation of the 3_1^- level in ^{88}Sr to the 2_1^+ level could be observed via a transition with E_γ = 898 keV. Due to the known branching ratio the contribution of the direct decay to the ground state could be estimated to be about 0.7% to 1.7%.

The nucleus ^{87}Rb has a ground-state spin of $J_0^\pi = \frac{3}{2}^-$. Consequently, the majority of states populated after the s-wave proton capture are those with $J^\pi = 1^-$ and 2^- decaying into the ground state with *E1* and *M2* transitions, respectively. The former is a likely decay and thus, the prompt γ decay to the ground state could be observed if the statistics in the γ-ray spectra were high enough. This was used as explained in Sec. 2 to approximate the offset of the accelerator since the direct decay of the compound nucleus to the ground state of ^{88}Sr, known as γ_0, could be observed for beam energies between E_p = 2.8 MeV and E_p = 5 MeV. A high energy spectrum for the measurement with a proton-beam of E_p = 3.5 MeV is shown in Fig. 4, where the γ_0 and other primary γ-rays to certain discrete states in ^{88}Sr are visible. In addition, this limits the uncertainty for the beam energy since with an approximated offset, $E_{c.m.}$ can be determined in two ways as explained.

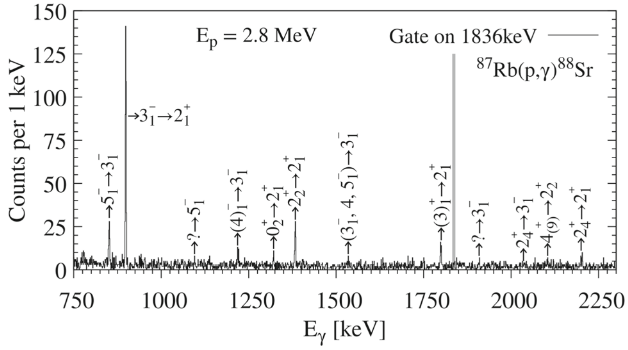

Fig. 5 Application of the $\gamma\gamma$-coincidence method on the ^{87}Rb(p, γ)^{88}Sr reaction for a proton-beam energy of $E_p = 2.8$ MeV. Gating on the $2_1^+ \rightarrow$ g.s. transition at $E_\gamma = 1836$ keV in the original spectrum reveals many transitions feeding this state. The width of the gate is marked with light grey lines. Different γ-ray cascades of higher lying states that de-excite into the 2_1^+ level can be identified. They are labeled in the figure

With the NuDAQ system [23] single spectra as well as $\gamma\gamma$-coincidence matrices can be generated. The latter are used to identify γ-ray cascades and consequently correlate these γ-ray transitions to a certain isotope. Further details on the used hardware and software for the analysis can be found in Ref. [23].

Moreover, they can be used to reduce beam-induced background and identify γ-ray transitions buried in the Compton background and estimate the intensity of these transitions. An example of the application of the $\gamma\gamma$-coincidence method with a gate on the $2_1^+ \rightarrow$ g.s. transition at $E_\gamma = 1836$ keV for a proton-beam energy of $E_p = 2.8$ MeV is shown in Fig. 5. As explained before, there is a noticeable background reduction such that the population of the different states can be observed in detail.

3.2 Angular Distribution

The total cross-section of the (p,γ) reaction is given by

$$\sigma_{(\mathrm{p},\gamma)_{\mathrm{tot}}} = \frac{N_{(\mathrm{p},\gamma)}}{N_p \cdot N_{T_1}}, \tag{6}$$

where $N_{(\mathrm{p},\gamma)}$ is the number of proton capture reactions, N_p is the number of projectiles and N_{T_1} is the number of target nuclei per area. The de-excitation of the highly excited compound nucleus occurs via the emission of γ rays, which follow an angular distribution $W(\theta)$ with respect to the beam axis [26]. This angular distribution $W(\theta)$ was sampled by groups of detectors placed at five different angles relative to the beam axis. The experimental yield of each detector group was determined as follows:

$$W(\theta) = \frac{Y(E_\gamma)}{\epsilon(E_\gamma) \cdot \tau}, \tag{7}$$

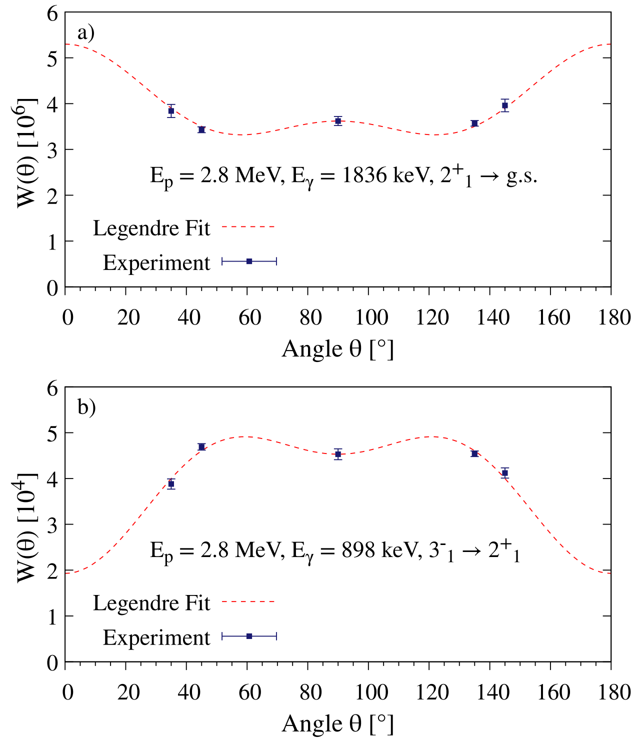

Fig. 6 The de-excitation of the highly excited compound nucleus via γ rays follows an angular distribution. The experimental yield is measured at five different angles and a sum of Legendre polynomials it fitted to it. The upper figure a) shows the measured angular distribution $W(\theta)$ for the $2_1^+ \rightarrow$ g.s. transition, whereas the lower figure b) shows the measured angular distribution $W(\theta)$ for the $3_1^- \rightarrow 2_1^+$ transition in ^{88}Sr for a proton-beam energy of $E_p = 2.8$ MeV

where $Y(E_\gamma)$ is the total number of detected γ-rays of energy E_γ at the angle θ, $\epsilon(E_\gamma)$ is the full-energy peak efficiency and τ is the dead time correction of the data acquisition.

A sum of Legendre polynomials is fitted to the experimental values in order to obtain the angular distribution

$$W(\theta) = A_0 \cdot \left(1 + \sum_{k=2,4} \alpha_k P_k(\cos(\theta))\right) \tag{8}$$

and especially its integral A_0. The angular distributions for all γ-ray transitions at each beam energy are obtained. Figure 6 shows the experimentally determined angular distributions $W(\theta)$ for the $2_1^+ \rightarrow$ g.s. and the $3_1^- \rightarrow 2_1^+$ transitions in ^{88}Sr for a proton-beam energy of $E_p = 2.8$ MeV at five different angles.

4 Results and Analysis

The different measured contributions to the population of the ground state can be seen in Fig. 7. For this, all A_0 coefficients of Eq. (8) for one beam energy for the observed ground state

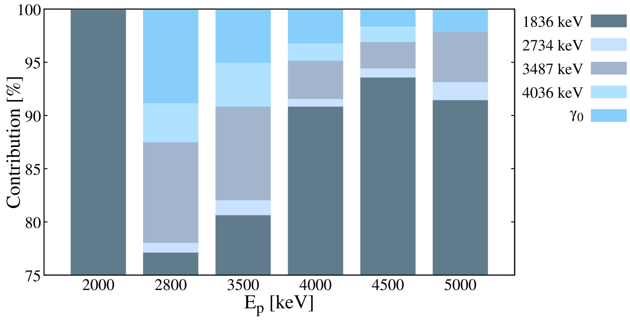

Fig. 7 The different contributions to the population of the ground state from different excited states of the ^{87}Rb(p, γ)^{88}Sr reaction at the six beam energies. Between 80% and 95% of the observed population of the ground state originate from the $2_1^+ \rightarrow$ g.s. transition at $E_\gamma = 1836$ keV. Note that for $E_p = 2.0$ MeV only the $2_1^+ \rightarrow$ g.s. transition was visible in the spectra due to low statistics. Therefore, only a reliable lower limit can be given

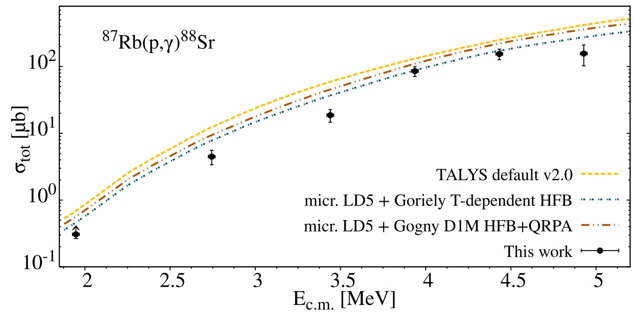

Fig. 8 Total experimental cross-section values $\sigma_{tot,exp}$ for the ^{87}Rb(p, γ)^{88}Sr reaction obtained in this work (black circles). For more details see text. The results are compared to different statistical model calculations using the TALYS 2.0 code [24]. The microscopic level density from the combinatorial model by Hilaire and Goriely [28] and two different photo strength functions [29,30] have been used in addition to the TALYS 2.0 default to compare experimental data to calculations. The different models are in fair agreement with the measured cross-section values

transitions are summed. This represents the total number of proton captures $N_{(p,\gamma)}$. As expected from the funnel effect [27], the contribution of the $2_1^+ \rightarrow$ g.s. transition yields the greatest contribution to the total cross section since many high-lying levels de-excite via γ-ray cascades that end up in the 2_1^+ state, which de-excites with $E_\gamma = 1836$ keV to the ground state. Since the 2_1^+ state is populated by a considerable contribution of different γ-ray cascades, the decay into the ground state shows a more or less isotropic behavior and the effect of the angular correlation is rather small as can be seen in Fig. 6 a). Due to the very low cross section at a E_p = 2 MeV, statistics are only sufficient to observe the $2_1^+ \rightarrow$ g.s. transition. Considering the trend in Fig. 7, we have to assume that about 25% of the produced ^{88}Sr nuclei de-excite via different ground-state transitions and therefore cannot be accounted for. Consequently, the cross section determined at this energy is a lower limit.

4.1 Total cross-section values

The measured total cross-section values obtained in this work are listed in the second column in Tab. 2. The uncertainties of the experimentally obtained cross-section values $\sigma_{\text{tot,exp}}$ are influenced by the uncertainties of the number of projectiles ($\approx$ 5%), the target thickness ($\approx$ 10%), the full-energy peak efficiency ($\approx 0.5 - 11\%$) and the statistical uncertainty for the fit of the Legendre polynomials ($\approx 1-10\%$). It should be noted that some of these uncertainties are energy dependent. Until now there are no other reported experimental data on this reaction. Figure 8 shows the results of this work in comparison with different statistical model calculations using the TALYS 2.0 code [24].

Table 2 Total experimentally obtained cross-section values $\sigma_{tot,exp}$ for the ^{87}Rb(p, γ)^{88}Sr reaction depending on the center-of-mass energy $E_{c.m.}$. For the beam energies between E_p = 2.8 MeV and E_p = 4.5 MeV five ground-state transitions have been observed, for the beam energy of E_p = 5.0 MeV four ground-state transitions have been observed, and for the beam energy of E_p = 2.0 MeV only the $2_1^+ \rightarrow$ g.s. transition with E_γ = 1836 keV has been observed. The single cross-sections for the observed ground-state decays are listed for each observed de-excitation. In the scope of TALYS calculations using version 2.0, the cross-section of the de-excitation $2_1^+ \rightarrow$ g.s. has been calculated [24] and is listed in the fourth column. For this calculation the microscopic level density from the combinatorial model by Hilaire and Goriely [28] and the temperature-dependent Skyrme-Hartree-Fock-Bogoliubov model [29] have been used

$E_{c.m.}$ [MeV]	$\sigma_{\text{tot,exp}}[\mu b]$	$\sigma_{1836\text{keV}}[\mu b]$	$\sigma_{\text{TALYS},2_1^+}[\mu b]$	$\sigma_{2734\text{keV}}[\mu b]$	$\sigma_{3485\text{keV}}[\mu b]$	$\sigma_{4035\text{keV}}[\mu b]$	$\sigma_{\gamma 0}[\mu b]$
1.947(23)	0.307(41)*	0.307(41)	0.298				
2.744(23)	4.5(11)	3.45(39)	5.27	0.041(5)	0.42(5)	0.164(33)	0.39(6)
3.440(22)	18.7(40)	15.1(17)	28.9	0.26(3)	1.64(20)	0.77(10)	0.93(18)
3.936(22)	85(14)	78(8)	70.9	0.61(7)	3.06(34)	1.38(18)	2.7(4)
4.432(22)	154(27)	144(26)	135	1.31(14)	3.82(50)	2.24(29)	2.4(4)
4.928(22)	156(54)	143(17)	207	2.6(3)	7.4(24)		3.3(5)

* lower limit

4.2 Statistical model analysis and discussion

The results of the calculations and their outcome depends mainly on the selected models for the nuclear input parameters. The most important input parameters are the nuclear level density (NLD) and the γ-ray strength function (γ-SF), which contain fundamental information about nuclear structure and decay behavior. As sensitivity studies as performed in Ref. [9] show, the ^{87}Rb(p, γ)^{88}Sr reaction is very sensitive to the γ-width, which is derived from the γ-SF. In the TALYS 2.0 code [24], a variety of models for NLD and γ-SF are implemented. The following models have been selected since they are reliable and have proven their predictive power in previous studies [31–34]: The microscopic level density stems from the combinatorial model by Hilaire and Goriely [28]. Two different photon strength functions have been chosen, namely the temperature-dependent Skyrme-Hartree-Fock-Bogoliubov model [29] and the Gogny-Hartree-Fock-Bogoliubov model [30].

The experimental cross-section values $\sigma_{tot,exp}$ for the ^{87}Rb(p, γ)^{88}Sr reaction obtained in this work are presented in Fig. 8 together with different statistical model calculations utilising the TALYS 2.0 [24] code. The models employed for the level-density and the γ-SF have been selected in accordance to the above mentioned criteria. The different models are in fair agreement with the experimentally determined cross-section values. The choice of the NLD and the γ-SF deviating from the TALYS 2.0 [24] default seem to improve the agreement slightly. All calculations seem to overestimate the cross sections at lower beam energies.

In addition to these calculations, the cross-section of different levels de-exiting to the ground state have been calculated using the TALYS 2.0 code [24] utilizing the microscopic level density from the combinatorial model by Hilaire and Goriely [28] and the temperature-dependent Skyrme-Hartree-Fock-Bogoliubov model [29]. These calculated cross-sections are compared to the measured cross-sections tabulated in Tab. 2 and shown in Fig. 9. The comparison shows that the TALYS 2.0 code [24] predictions for the different observed levels for the cross-sections are in fair agreement. Furthermore, TALYS [24] predicts additional de-excitations from discrete level to the ground-state. This is especially interesting since the states at $E_x = 3378$ keV and $E_x = 3485$ keV are located at a similar energy and show a similar cross-section for the decay to the ground-state, but experimentally only the de-excitation of $E_x = 3485$ keV to the ground-state was observed. Similar applies for the following levels: $E_x = 3218$ keV, $E_x = 3522$ keV, $E_x = 4035$ keV, $E_x = 4226$ keV and $E_x = 4262$ keV. They all share a similar calculated cross-section σ_{E_γ} and for some similar energy for the decay to the ground-state, however, only the de-excitation to the ground-state of $E_x = 4035$ keV was observed in the experiment. This indicates that the calculations using the TALYS 2.0 code [24] cannot reproduce the experimental observations. It seems that TALYS takes too many ground-state decays into account for the cross-section calculation. Moreover, as shown in Fig. 4 for $E_p = 3.5$ MeV no primary γ-rays have been observed to discrete levels that the TALYS 2.0 code [24] predicts in addition to the observed levels, that de-excite to the ground-state.

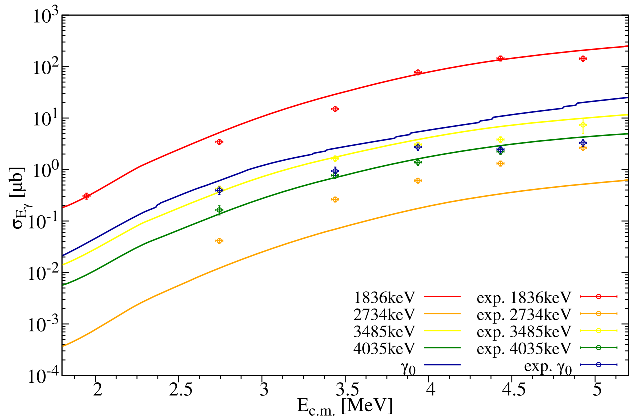

Fig. 9 The cross-sections of different levels de-exciting to the ground-state from calculations using the TALYS 2.0 code [24] utilizing the microscopic level density from the combinatorial model by Hilaire and Goriely [28] and the temperature-dependent Skyrme-Hartree-Fock-Bogoliubov model [29] compared to the measured cross-sections σ_{E_γ} of the observed de-excitations. The measured and calculated cross-sections σ_{E_γ} are in fair to good agreement, depending on the de-exciting level E_x. The trend for the different energies $E_{c.m.}$ is reproduced well for most of the energies E_γ

Previous studies of ^{92}Mo and ^{88}Sr showed deviations for the low-energy part of the measurement, too, as shown in Fig. 10. Therefore, a re-evaluation of the NLD and the γ-SF in this region could be useful to better understand the production mechanisms of ^{92}Mo and ^{92}Nb. Most likely, no enhancement in the low-energy limit is observed in the γ-SF for ^{88}Sr. This is in contrast to ^{94}Mo, where the low-energy enhancement is required [32].

5 Summary and conclusion

In this work, the total cross-sections of the ^{87}Rb(p, γ)^{88}Sr reaction have been studied experimentally at six proton-beam energies between $E_p = 2$ MeV to 5 MeV for the first time. By studying the radiative proton-capture on ^{87}Rb the nuclear physics characteristics of ^{88}Sr can be accessed. It has been demonstrated that the employed level-density model from the combinatorial model by Hilaire and Goriely [28] provides decent predictions regarding ^{88}Sr. The total cross sections for the ^{87}Rb(p, γ)^{88}Sr reaction can be described by statistical model calculations using the previously mentioned set of parameters. It was concluded that a possible low-energy

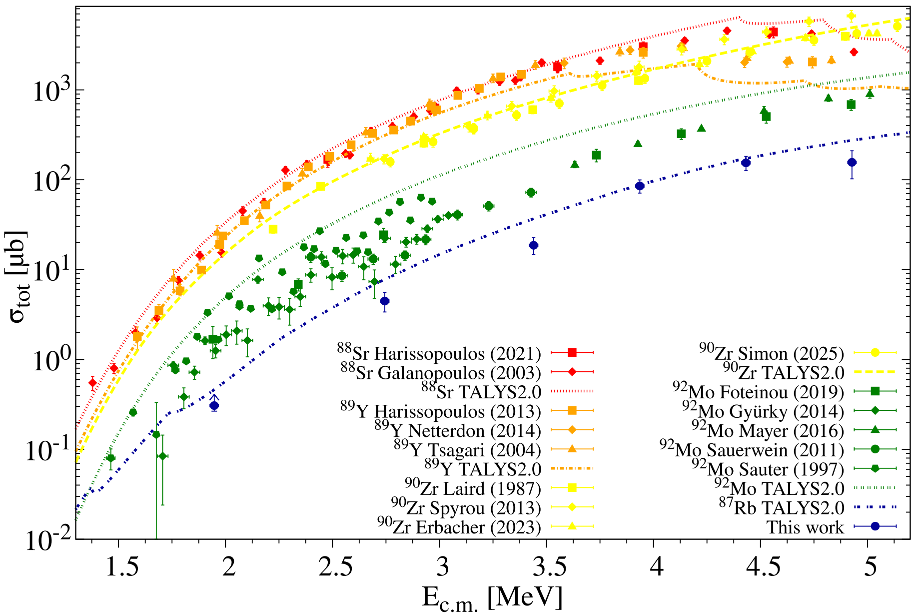

Fig. 10 Comparison between different measured total cross section values σ_{tot} for (p, γ) reactions on the following nuclei in the $N = 50$ isotonic chain: ^{87}Rb (This work), ^{88}Sr [35,36], ^{89}Y [37–39], ^{90}Zr [40–43], and ^{92}Mo [44–48]. The results are compared to statistical model calculations using the TALYS 2.0 code [24], where the microscopic level density from the combinatorial model by Hilaire and Goriely [28] and the photo strength function from Ref. [29] have been used

enhancement of the γ-SF in ^{88}Sr would have at most a negligible effect on the cross-section values. A more systematic comparison between the various measured cross-sections of the stable N = 50 nuclei as shown in Fig. 10 can deepen the understanding of the underlying nuclear physics and can help to improve the underlying models for the statistical model calculations within a certain mass region. Therefore, a comparison of cross-sections and the robustness of the used models for the ^{87}Rb(p, γ)^{88}Sr reaction with the ^{85}Rb(p,γ)^{86}Sr reaction is planned. The influence of the obtained cross sections $\sigma_{tot,exp}$ on the stellar reactions rates will be studied in detail in the future.

Acknowledgements We gratefully thank A. Blazhev for the target preparation and F. Heim for discussion. The authors thank the accelerator team at the Institute for Nuclear Physics in Cologne. This project has been supported by the Deutsche Forschungsgemeinschaft under the contracts ZI 510/12-1. SW is supported by the Hans-Böckler-Stiftung.

Author contributions All authors contributed to the study conception and design. Material preparation, data collection and analysis were performed by Svenja Wilden, Martin Müller, and Benedikt Machliner. The first draft of the manuscript was written by Svenja Wilden and all authors commented on previous versions of the manuscript. All authors read and approved the final manuscript.

Funding Open Access funding enabled and organized by Projekt DEAL. This project has been supported by the Deutsche Forschungsgemeinschaft under the contract ZI 510/12-1 (project 544767130). SW is supported by the Hans-Böckler-Stiftung.

Data Availability Statement Data sets generated and/or analyzed during the current study are available from the corresponding author on reasonable request.

Code Availability Statement This manuscript has no associated code/software.

Declarations

Conflict of interest The authors have no conflict of interest to declare that are relevant to the content of this article.

References

1. E.M. Burbidge, G.R. Burbidge, W.A. Fowler, F. Hoyle, Rev. Mod. Phys. **29**(4), 547 (1957)
2. S.E. Woosley, W.M. Howard, Astrophys. J. Suppl. **36**, 285 (1978). https://doi.org/10.1086/190501
3. M. Arnould, S. Goriely, Phys. Rep. **384**, 1 (2003). https://doi.org/10.1016/S0370-1573(03)00242-4
4. M. Arnould, S. Goriely, Prog. Part. Nucl. Phys. **112**, 103766 (2020). https://doi.org/10.1016/j.ppnp.2020.103766
5. C. Fröhlich, G. Martínez-Pinedo, M. Liebendörfer, F.-K. Thielemann, E. Bravo, W.R. Hix, K. Langanke, N.T. Zinner, Phys. Rev. Lett. **96**, (2006). https://doi.org/10.1103/physrevlett.96.142502

6. T. Rauscher, N. Dauphas, I. Dillmann, C. Fröhlich, Z. Fülöp, G. Gyürky, Rep. Prog. Phys. **76**, 066201 (2013). https://doi.org/10.1088/0034-4885/76/6/066201
7. A. Choplin, S. Goriely, R. Hirschi, N. Tominaga, G. Meynet, Astron. Astrophys. **661**, 86 (2022). https://doi.org/10.1051/0004-6361/202243331
8. W. Rapp, J. Gorres, M. Wiescher, H. Schatz, F. Kappeler, Astrophys. J. **653**, 474–489 (2006). https://doi.org/10.1086/508402
9. T. Rauscher, Astrophys. J. Suppl. **201**, 26 (2012). https://doi.org/10.1088/0067-0049/201/2/26
10. M. Tessler, J. Zappala, S. Cristallo, L. Roberti, M. Paul, S. Halfon, T. Heftrich, W. Jiang, D. Kijel, A. Kreisel, M. Limongi, Z.-T. Lu, P. Müller, R. Purtschert, R. Reifarth, A. Shor, D. Veltum, D. Vescovi, M. Weigand, L. Weissman, Phys. Rev. C **104**, 015806 (2021). https://doi.org/10.1103/PhysRevC.104.015806
11. L. Roberti, M. Limongi, A. Chieffi, Astrophys. J. Suppl. **270**, 28 (2024). https://doi.org/10.3847/1538-4365/ad1686
12. Roberti, L. Private communication (2025)
13. F. Heim, J. Mayer, M. Müller, P. Scholz, M. Weinert, A. Zilges, Nucl. Instrum. Methods A **966**, 163854 (2020). https://doi.org/10.1016/j.nima.2020.163854
14. Chu, W.-K., Mayer, J., Nicolet, M.-A. Backscattering Spectrometry. Academic Press, Inc., Heidelberg (1978). https://doi.org/10.1016/B978-0-121-73850-1.X5001-7
15. RUBION - Zentrale Einrichtung für Ionenstrahlen und Radionuklide. https://www.rubion.rub.de/methods/41/
16. M. Mayer, *SIMNRA User's Guide, Report IPP 9/113* (Max-Planck-Institut für Plasmaphysik, Garching, Germany, 1997)
17. M. Wang, W.J. Huang, F.G. Kondev, G. Audi, S. Naimi, Chin. Phys. C **45**, 030003 (2021). https://doi.org/10.1088/1674-1137/abddaf
18. J. Ziegler, J. Biersack, and M. Ziegler, SRIM – The Stopping and Range of Ions in Matter. http://srim.org/
19. E.A. McCutchan, A.A. Sonzogni, Nucl. Data Sheets **115**, 135 (2014). https://doi.org/10.1016/j.nds.2013.12.002
20. H. Junde, H. Su, Y. Dong, Nucl. Data Sheets **112**, 1513 (2011). https://doi.org/10.1016/j.nds.2011.04.004
21. E. Browne, J.K. Tuli, Nucl. Data Sheets **111**, 1093 (2010). https://doi.org/10.1016/j.nds.2010.03.004
22. CAEN S.p.A. - *User Manual UM6875 - V1782 Octal Digital MCA*. http://www.caen.it/products/v1782/
23. Weinert, M. Investigation of Microscopic Structures in the Low-Energy Electric Dipole Response of 120Sn using Consistent Experimental and Theoretical Observables and Digital Signal Processing for Nuclear Physics Experiments. PhD thesis, University of Cologne (2022)
24. Koning, A., Hilaire, S., Goriely, S. Eur. Phys. J. A **59** (2023) https://doi.org/10.1140/epja/s10050-023-01034-3
25. Johnson, T.D., Kulp, W.D. Nucl. Data Sheets **129** (2015) https://doi.org/10.1016/j.nds.2015.09.001
26. T. Mayer-Kuckuk, *Kernphysik*, 4th edn. (Teubner Studienbücher. Vieweg & Teubner, Wiesbaden, Germany, 1984)
27. A. Zilges, D.L. Balabanski, J. Isaak, N. Pietralla, Prog. Part. Nucl. Phys. **122**, 103903 (2022). https://doi.org/10.1016/j.ppnp.2021.103903
28. S. Goriely, S. Hilaire, A.J. Koning, Phys. Rev. C **78**, 064307 (2008). https://doi.org/10.1103/PhysRevC.78.064307
29. S. Goriely, E. Khan, M. Samyn, Nucl. Phys. A **739**, 331 (2004). https://doi.org/10.1016/j.nuclphysa.2004.04.105
30. S. Goriely, S. Hilaire, S. Péru, K. Sieja, Phys. Rev. C **98**, 014327 (2018). https://doi.org/10.1103/PhysRevC.98.014327
31. Wiedeking, M., Goriely, S. Philos. Trans. R. Soc. A **382** (2024) doi:https://doi.org/10.1098/rsta.2023.0125
32. Heim, F., Scholz, P., Mayer, J., Müller, M., Zilges, A. Phys. Rev. C. **101** (2020) https://doi.org/10.1103/PhysRevC.101.035807
33. Heim, F., Scholz, P., Körschgen, M., Mayer, J., Müller, M., Zilges, A. Phys. Rev. C. **101** (2020) https://doi.org/10.1103/PhysRevC.101.035805
34. Heim, F., Mayer, J., Müller, M., Scholz, P., Zilges, A. Phys. Rev. C. **103** (2021) https://doi.org/10.1103/PhysRevC.103.055803
35. S. Harissopulos, E. Vagena, P. Dimitriou, M. Axiotis, S. Galanopoulos, V. Foteinou, A. Lagoyannis, Phys. Rev. C **104**, 025804 (2021). https://doi.org/10.1103/PhysRevC.104.025804
36. S. Galanopoulos, P. Demetriou, M. Kokkoris, S. Harissopulos, R. Kunz, M. Fey, J.W. Hammer, G. Gyürky, Z. Fülöp, E. Somorjai, S. Goriely, Phys. Rev. C **67**, 015801 (2003). https://doi.org/10.1103/PhysRevC.67.015801
37. S. Harissopulos, A. Spyrou, A. Lagoyannis, M. Axiotis, P. Demetriou, J.W. Hammer, R. Kunz, H.-W. Becker, Phys. Rev. C **87**, 025806 (2013). https://doi.org/10.1103/PhysRevC.87.025806
38. L. Netterdon, V. Derya, J. Endres, C. Fransen, A. Hennig, J. Mayer, C. Müller-Gatermann, A. Sauerwein, P. Scholz, M. Spieker, A. Zilges, Nucl. Instrum. Methods Phys. Res. A **754**, 94–100 (2014). https://doi.org/10.1016/j.nima.2014.04.025
39. P. Tsagari, M. Kokkoris, E. Skreti, A.G. Karydas, S. Harissopulos, T. Paradellis, P. Demetriou, Phys. Rev. C **70**, 015802 (2004). https://doi.org/10.1103/PhysRevC.70.015802
40. C.E. Laird, D. Flynn, R.L. Hershberger, F. Gabbard, Phys. Rev. C **35**, 1265–1274 (1987). https://doi.org/10.1103/PhysRevC.35.1265
41. A. Spyrou, S.J. Quinn, A. Simon, T. Rauscher, A. Battaglia, A. Best, B. Bucher, M. Couder, P.A. DeYoung, A.C. Dombos, X. Fang, J. Görres, A. Kontos, Q. Li, L.Y. Lin, A. Long, S. Lyons, B.S. Meyer, A. Roberts, D. Robertson, K. Smith, M.K. Smith, E. Stech, B. Stefanek, W.P. Tan, X.D. Tang, M. Wiescher, Phys. Rev. C **88**, 045802 (2013). https://doi.org/10.1103/PhysRevC.88.045802
42. Erbacher, P., Heftrich, T., Endres, A., Glorius, J., Netterdon, L., Just, D., Göbel, K., Krtička, M., Reifarth, R., Sonnabend, K., Thomas, B., Weigand, M., Zilges, A. Eur. Phys. J. A **59**(4) (2023) https://doi.org/10.1140/epja/s10050-023-00984-y
43. Simon, A., Koros, J., Olivas-Gomez, O., Kelmar, R., Churchman, E., Clark, A.M., Harris, C., Henderson, S.L., Kelly, S.E., Millican, P., Palmisano-Kyle, A., Reingold, C.S., Robertson, D., Stech, E., Spyrou, A., Tan, W.P. Eur. Phys. J. A **61**(3) (2025) https://doi.org/10.1140/epja/s10050-025-01521-9
44. Foteinou, V., Axiotis, M., Harissopulos, S., Dimitriou, P., Provatas, G., Lagoyannis, A., Becker, H.-W., Rogalla, D., Zilges, A., Schreckling, A., Endres, A. Eur. Phys. J. A **55**(5) (2019) https://doi.org/10.1140/epja/i2019-12738-x
45. G. Gyürky, M. Vakulenko, Z. Fülöp, Z. Halász, G.G. Kiss, E. Somorjai, T. Szücs, Nucl. Phys. A **922**, 112–125 (2014). https://doi.org/10.1016/j.nuclphysa.2013.12.003
46. Mayer, J., Goriely, S., Netterdon, L., Péru, S., Scholz, P., Schwengner, R., Zilges, A. Phys. Rev. C. **93** (2016) https://doi.org/10.1103/PhysRevC.93.045809
47. A. Sauerwein, M. Elvers, J. Endres, J. Hasper, A. Hennig, L. Netterdon, A. Zilges, P. Demetriou, R. Julin, S. Harissopulos, AIP Conf. Proc. **1377**, 423–425 (2011). https://doi.org/10.1063/1.3628433
48. T. Sauter, F. Käppeler, Phys. Rev. C **55**, 3127–3138 (1997). https://doi.org/10.1103/PhysRevC.55.3127